Heterogeneous Phototransformation of Halogenated Polycyclic Aromatic Hydrocarbons: Influencing Factors, Mechanisms and Products

Yueyao Yang[1, 2, 3], Yahui Liu[1, 2, 3], Guohua Zhu[2], Bingcheng Lin[2], Shanshan Zhang[1, 2, 3], Xin Li[1, 2, 3], Fangxi Xu[4], He Niu[4], Rong Jin[2, *], Minghui Zheng[1, 2, 3]

[1] State Key Laboratory of Environmental Chemistry and Ecotoxicology, Research Center for Eco-Environmental Sciences, Chinese Academy of Sciences, Beijing, 100085, China

[2] School of Environment, Hangzhou Institute for Advanced Study, University of Chinese Academy of Sciences, Hangzhou, 310024, China

[3] College of Resource and Environment, University of Chinese Academy of Sciences, Beijing, 100049, China

[4] Zhejiang Taizhou Ecological and Environmental Monitoring Center, Taizhou 318000, China

* Correspondence to: jinrong@ucas.ac.cn (R. Jin)

ABSTRACT

Chlorinated and brominated polycyclic aromatic hydrocarbons (XPAHs) are emerging pollutants widely found in atmospheric particulate matter (PM). However, their environmental transformation mechanisms remain poorly understood. In this study, we collected PM samples of varying sizes over a year for XPAH analysis and found that the average concentrations of XPAHs peaked in winter and were dominated by the contribution of PM_1 (47.0%). Correlation analysis with relevant meteorological parameters showed strong associations between XPAH fluctuations and PM, temperatures, and humidity. Hence, controlled laboratory experiments were conducted to explore the influence of particle size, sunlight duration, temperature, humidity, and oxidant concentrations on XPAHs. Our results indicated that the transformation rates of XPAHs were influenced by the parent polycyclic aromatic hydrocarbon structures, with phenanthrene < fluoranthene < pyrene < benz[a]anthracene ≈ anthracene < benzo[a]pyrene, as well as the substitution of halogens: chlorinated < brominated. Furthermore, the photo irradiation promoted the heterogeneous transformation of XPAHs; this process was accelerated by the increased concentrations of reactive oxygen species and elevated temperature, peaking at the humidity level of 45%. The transformation products were identified by nontarget analysis. Accordong to that, we then proposed phototransformation pathways for XPAHs, suggesting a mechanism involving dehalogenation followed by oxidation. Predictions were made regarding the persistence, bioaccumulation, long-range transportation, and toxicities of XPAHs and their transformation products, showing a decrement in environmental risks as the transformation progressed. This study provides novel insights into the primary influencing factors for particulate XPAH variations and the mechanisms of heterogeneous phototransformation.

KEYWORDS: Photochemistry; Influencing factors; Heterogeneous phototransformation; Transformation mechanism; Transformation pathways;

1. Introduction

Chlorinated and brominated polycyclic aromatic hydrocarbons (ClPAHs and BrPAHs), cumulatively referred to as XPAHs, are halogenated derivatives of polycyclic aromatic hydrocarbons (PAHs) that have gained considerable attention in recent years due to their heightened persistence, toxicity, and bioaccumulation relative to their parent PAHs (Jin et al. 2017b; Ma et al. 2013; Nishimura et al. 2017; Ohura et al. 2013). At present, research on XPAHs primarily encompasses the following aspects: (1) Establishment of pre-treatment and instrumental methods (Jin et al. 2023; Liu et al. 2019b; Noro et al. 2023; Sei et al. 2021; Takikawa et al. 2023), (2) Environmental detection across various environmental media (Jin et al. 2020; Xie et al. 2021), and (3) Identification of anthropogenic sources. XPAHs have been reported to exist in the air (Jin et al. 2017c; Kakimoto et al. 2014; Nilsson and Ostman 1993), soil (Sun et al. 2013; Zhang et al. 2006), water (Shiraishi et al. 1985), sediment (Ohura et al. 2015), and organisms (Jin et al. 2017a; Liu et al. 2019b; Nishimura et al. 2017; Ohura et al. 2015; Xia et al. 2019). The sources, such as industrial thermal processes (Yang et al. 2022b), electronic waste decomposition (Wang et al. 2022), and vehicular emissions (Deng et al. 2023) have been identified, by means of detection of XPAHs in the stack gas and fly ash emitted from these sources (Jin et al. 2017b; Nishimura et al. 2017; Yang et al. 2022a). However, a significant aspect of research appears to have been overlooked: i.e., the environmental transformation. Variations in the transformation mechanisms of XPAH congeners in environmental matrices can result in differences in their environmental fate and associated risks.

The photochemical processes have been verified to represent a marked elimination pathway for organic substances affecting the atmosphere (Hu et al. 2021; Laskin et al. 2015; Malecha and Nizkorodov 2016). For example, PAHs have been confirmed to undergo oxidation (Zhu et al. 2022), or thorough fragmentation (Hu et al. 2021; Zhang et al. 2024) under atmospheric photochemical reactions. Therefore, despite the absence of direct study, given their structural similarities to PAHs, XPAHs also possess the potential to undergo similar processes. Studies by Ohura et al. also confirmed the photochemical transformation of ClPAHs when being exposed to light in cyclohexane solvent (Ohura et al. 2008). Field observations provided additional evidence suggesting that the photochemistry plays a crucial role in atmospheric XPAH transformation. For instance, certain studies have shown that concentrations of ClPAHs in particulate matter (PM) were slightly higher during nighttime than during daytime (Ma et al. 2013; Ohura et al. 2013), indicating that daytime photochemistry contributed to the

transformation of XPAHs. For BrPAHs, although no direct nighttime versus daytime concentration comparison has been conducted, prior research indicated that BrPAHs might exhibit greater instability under photo irradiation than ClPAHs (Ohura et al. 2009).

Heterogeneous reactions were identified to be the key mechanisms driving the transformation of atmospheric organic compounds, e.g., PAHs (Jia et al. 2019), during these photochemistry processes (Zhang et al. 2023). Atmospheric PM acts as a significant carrier for both environmental pollutants and catalysts, serving as a medium for heterogeneous reactions. These reactions could be influenced by various environmental factors. For instance, the reactive oxygen species (ROS) have been identified to accelerate the phototransformation of polychlorinated naphthalene (PCNs), which are two-ring ClPAHs, on the surface of silica gel (Kang et al. 2021). In addition, the temperature and humidity have been noted to influence the lifetime of atmospheric organics (Shiraiwa et al. 2011). For example, the heterogeneous oxidation mechanisms of organophosphate flame retardants were found to be significantly affected by humidity (Liu et al. 2019a). In the case of particulate XPAHs, heterogeneous reactions may also play a crucial role in their transformation. However, the influencing factors, specific mechanisms, pathways, and products remain unclear, necessitating further exploration.

This study aims to unravel the mechanisms, influencing factors, pathways, and products of XPAH heterogeneous transformation on PM. To achieve this, we conducted field studies complemented by meticulously designed laboratory experiments and nontarget organic compound analysis. Initially, we collected year-range particle samples of various sizes along with relevant meteorological data. These samples were subsequently analyzed for XPAHs. Through multivariate parameter analysis, we explored XPAH fluctuations correlated with meteorological data to pinpoint key influencing factors. Subsequently, controlled laboratory experiments were designed and conducted to unveil the heterogeneous transformation of XPAHs under the influence of particle size, humidity, temperature, and atmospheric oxidant content. The persistence, bioaccumulation, long-range transportation, and toxicities of the transformation products were then assessed to determine the environmental risks associated with XPAH transformation. Therefore, the findings of this study contribute comprehensive insights into the mechanisms and environmental risks involved in the fate of XPAHs in the environment.

2. Materials and methods

2.1 Experimental materials

In this study, a comprehensive investigation was conducted on 41 XPAHs with 2 to 5 benzene rings,

along with an analysis of the corresponding parent PAHs. The parent PAHs are abbreviated as follows: Nap (naphthalene), Phe (phenanthrene), Ant (anthracene), Triph (triphenylene), Fluor (fluoranthene), Pyr (pyrene), BaA (benz[a]anthracene), and BaP (benzo[a]pyrene). The congeners in the ClPAH and BrPAH groups are described as Cl-, Cl_2-, Cl_3-, Cl_4-, Br-, and Br_2-, indicating the presence of monochlorinated, dichlorinated, trichlorinated, tetrachlorinated, monobrominated, and dibrominated PAH derivatives, respectively, with the numbers denoting the substituting positions. Specific names, abbreviations, and molecular structures of 20 ClPAHs and 21 BrPAHs are listed in **Table S1**. As reported in our previous study (Jin et al. 2017c), standards, isotopically labeled internal standards, and recovery standards for XPAHs and PAHs were commercially obtained.

2.2 Sample collection and extraction

Atmospheric particles of three sizes (PM_1, $PM_{2.5}$, PM_{10}) were collected in Hangzhou from March 2023 to February 2024 using medium-flow samplers (Wuhan Tianhong Instruments Co., Ltd., China). These samplers were positioned atop a school building at a height of approximately 15 meters above ground level. The sampling site (30° 8′ 15" N, 120° 4′ 17" E) was situated in the Xihu District of Hangzhou, with no industrial area within a five-kilometer radius. Samples were collected in monthly cycles, at a flow rate of 0.1 m^3/min. Quartz fiber filters were employed to capture particles. Subsequently, samples were collected, dried, weighed, and stored at −18 ℃.

Samples were extracted with a mixture of dichloromethane and hexane (1:4, v: v) by an auto-Soxhlet extractor (Universal Extractor E-800, Buchi, Germany). The extracted samples were then purified using an active silica column and concentrated to 50 μL using a rotary evaporator and nitrogen blower. Specific processes for the extraction and clean-up processes can be found in our previous study (Jin et al. 2017c).

2.3 Experiments design for heterogeneous transformation of particulate XPAHs

In this study, we designed a photo-transformation device that provided complete confinement and precise control over the experimental conditions. The reaction unit employed a xenon lamp (light intensity: 100 $mW \cdot cm^{-2}$, luminous efficacy: 100 lm/W) as the primary light source with an AM1.5 filter, which can achieve a good fit with the sunlight spectrum, effectively simulating the outdoor solar radiation (the average luminous efficacy ranged from 100 to 120 lm/W at noon at the sampling sites) (Cao et al. 2020; Wang et al. 2020). The entire photolysis reaction unit comprises a gas supply, mass flowmeters, a dryer (with molecular sieve and color silica gel), a bubbler containing Milli-Q water, a

xenon lamp, an optical reactor, a quartz reaction vessel, a temperature control system, gas absorption bottles, and a relative humidity monitoring component (**Fig. 1a**). To accurately emulate atmospheric conditions, model particles and a composite mixture comprising 41 XPAHs were meticulously prepared. Sequentially, 20 μL of the XPAHs mixture (1 mg/L) or individual congener solution was deposited onto the surface of the prepared layer of silica particles (M_{XPAHs}: M_{PM} = 2μg/g) (**Fig. 1b** and **Fig. S1**). The settings of the concentrations were based on previous studies on the XPAH concentrations per particle mass (Jin et al. 2017a; Jin et al. 2018). Specific information on the devices and experiments are described in **Text S1**.

To comprehensively explore the impact of various factors, including particle sizes (100 nm, 2 μm, 10 μm), temperatures (10°C, 20°C, 30°C), humidity (RH=30%, 45%, 60%), oxidant concentrations (H_2O_2 was selected for its representativeness among reactive oxygen species and ease of control, 0’% (+ tert-butyl alcohol; TBA), 0%, 1%, 3%, 5%, 10%), and irradiation duration (0 min, 10 min, 30 min, 60 min, 180 min), on the phototransformation mechanism of XPAHs, a series of experiments were conducted (**Text S1)**. The reacted gas was directed into a toluene solution for analysis of XPAHs in the tail gas, with less than 1% of the XPAHs escaping through volatilization during the reaction time. Dark control groups were conducted in each experiment to ensure that the difference between the two sets of experiments was due to the transformation effect caused by photo irradiation. Upon completion of the reactions, the particle layer within the reaction vessel was sonicated with 200 μL of toluene, followed by centrifugation of the supernatant. The resulting solution was then transferred into a centrifuge tube for subsequent product analysis.

2.4 Instrumental analysis

Analysis of the XPAHs and PAHs was conducted using gas chromatography coupled with magnetic sector high-resolution mass spectrometry (HRGC-HRMS, DFS, Thermo Fisher Scientific, USA) equipped with an electron ionization source. Specific information on the parameters for the oven and MS can be found in our previous study (Jin et al. 2017a). The analytical program and instrumental parameters for the analysis of PAHs were set according to “CalEPA Method 429”.

Non-target analysis of the transformation products of XPAHs was performed using a Trace 1310 GC coupled to a quadrupole-Orbitrap MS (Thermo Fisher Scientific, USA). Data were collected and processed using Thermo Scientific TraceFinder 5.1 software. High-resolution mass spectra of unknown compounds were deconvoluted into pure spectra using the Deconvolution Plugin of TraceFinder

software and then verified against the standard mass spectra from the commercial library NIST 2014. Specific information on the non-target analysis was shown in **Text S2**.

2.5 Environmental behavior and toxicity assessment of XPAHs and their transformation products

To assess the ecological risk and environmental characteristics—specifically, persistence, long-range transport potential, and bioaccumulation—of transformation products of XPAHs, this study employed the KOWWIN, KOAWIN, BCFBAF, and Level III fugacity models within EPI Suite 4.1 to compute various physicochemical properties of compounds. Essential environmental parameters, including molecular weight, octanol-water partition coefficient (Kow), air-water partition coefficient (Kaw), and half-lives in air, water, and soil, were subsequently introduced into the Pov-LRTP tool (Concha and Manzano 2023). Subsequently, the P-B-LRTP score is developed based on persistence (Pov), characteristic travel distance (CTD), and transfer efficiency (TE) values to prioritize the screened compounds. The respiratory toxicity model in ProTox 3.0(Banerjee et al. 2024) was used to predict the toxicity of the products, assessing their median lethal dose (LD50) and toxicity class.

$$\mathrm{P-B-LRTP\ Score}_i = LogPov + LogBAF + LogTE$$

2.6 Quality assurance and quality control

For the analysis of actual atmospheric PM samples, the recovery rates of internal standards ranged from 52% to 105%. In laboratory simulation experiments, the recovery rates of XPAHs ranged from 78% to 115%, while those of PAHs ranged from 53% to 120%. These recovery rates met the requirements for the detection and analysis of persistent organic pollutants. The detection limits (LODs) ranged from 0.17 to 1.9 fg/m^3 for ClPAHs, and from 0.23 to 1.6 fg/m^3 for BrPAHs. The LODs for ClPAH or BrPAH monomers vary due to differences in chemical structures, properties, and substituents, which influence their stability, response, and signal intensity during analysis, ultimately affecting detection limits. A blank sample was analyzed together with each batch of samples, and the relative concentrations of all XPAH congeners were below the detection limits.

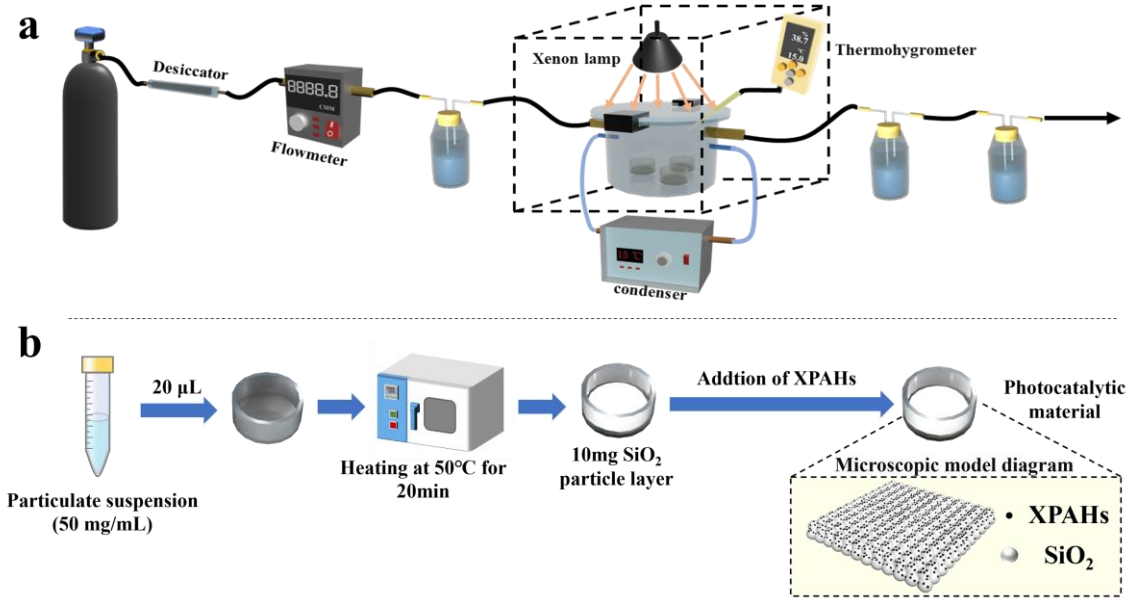

Fig. 1. (a) The laboratory photochemical transformation setup. (b) Particulate matter preparation process.

3. Results and discussion

3.1 Occurrence levels and congener profiles of particulate XPAHs

During the sampling period, PM concentrations ranged from 41.5 to 653 μg/m^3, with an average concentration of 130 μg/m^3 (**Fig. S2a**). PM_1 had the highest proportion, with an average of 47.0%, while the proportions of $PM_{1\text{-}2.5}$ and $PM_{2.5\text{-}10}$ were comparable. Notably, the peak concentration was recorded in April 2023. This surge coincided with a dust storm originating from the north, leading to heightened levels of suspended dust in the atmosphere and a significant spike in PM levels. Barring exceptional weather conditions, PM concentrations in other seasons were approximately twice as high as those observed in the summer and autumn.

The concentrations of $\sum_{21}$ClPAHs in the particles ranged from 0.6 to 61.5 pg/m^3 (mean: 12.1 pg/m^3), while those of $\sum_{18}$BrPAHs ranged from N.D. to 5.4 pg/m^3 (mean: 0.6 pg/m^3) during the sampling period (**Fig. 2a**). These values are lower than those reported in previous studies, such as Beijing, China ($\sum_{19}$ClPAHs: 128.8 pg/m^3, $\sum_{19}$BrPAHs: 9.5 pg/m^3) (Jin et al. 2017a); Ulsan, South Korea ($\sum_{11}$BrPAHs: 1.62 pg/m^3) (Vuong et al. 2020); and Shizuoka, Japan ($\sum_{20}$ClPAHs: 133.0 pg/m^3) (Ohura et al. 2013). For distribution in particles of different sizes, ClPAHs had the highest fraction in PM_1 (mean: 45.4%, range: 29.4–65.9%) and comparable proportions in $PM_{1\text{-}2.5}$ (mean: 28.1%, range: 13.0–52.0%) and $PM_{2.5\text{-}10}$ (mean: 26.5%, range: 8.46–3.5%). Conversely, BrPAHs showed no significant variance across the three particle size ranges, with concentrations of PM_1 (mean: 35.9%, range: 12.5–68.2%), $PM_{1\text{-}2.5}$ (mean: 35.7%, range: 14.3–55.2%) and $PM_{2.5\text{-}10}$ (mean: 28.4%, range: 1.25–59.2%) (**Fig. 2b**). In total,

over 70% of XPAHs were bound to particles with diameters smaller than 2.5 μm.

Concentration trends of XPAH homologue groups were as follows: ClFluor > ClBaP > ClAnt > ClPyr > ClPhe > ClBaA (**Table S2**); BrPyr > BrPhe > BrAnt > BrTriph > BrBaA > BrFluor (N.D.) (**Table S3**). The distribution profiles of XPAH congeners in PM_{10} in Hangzhou are shown in **Fig. S2b**, **Fig. S2c**, and **Table S4**. Among ClPAHs, 2-ClPhe/9-ClPhe, 1,5-Cl_2Ant/9,10-Cl_2Ant, 1-ClPyr, 3-ClFluor, 3,8-Cl_2Fluor, and 6-ClBaP were found to be predominant throughout the year. This distributions aligned with findings of prior studies (Jin et al. 2017a; Kitazawa et al. 2006; Ma et al. 2013). It is worth noting that 6-ClBaP, characterized by the highest molar mass and highest toxic equivalent factor investigated within ClPAHs investigated in our study, demonstrated the highest concentration proportion. BrPAHs are predominantly constituted by 2-BrPhe, 9-BrPhe, 7-BrBaA, and 1,6-Br_2Pyr. This represented a notable difference from previous literature which predominantly identified 3-BrFluor, 1,8-Br_2Ant, and 1-BrPyr as the primary congeners of BrPAHs in atmospheric PM in Beijing (Jin et al. 2017a). This disparity underscores variances in their respective sources or transformations.

3.2 Key environmental factors influencing temporal variations of particulate XPAHs

Extreme weather events such as sandstorms and prolonged light rainfall have been excluded in the following discussion. The average concentrations of PM and BrPAHs reached nadirs during summer and autumn while showing higher levels in the spring and winter (**Fig. S2d**). Conversely, ClPAH concentrations remained relatively stable during the spring and the summer, decreased in the autumn, and peaked in the winter. The seasonal characteristics of ClPAHs with different parent PAH structures also varied (**Fig. 2c**). Except for ClBaA, the remaining ClPAHs reached their highest concentrations during the winter. ClFluor showed elevated concentrations in both the spring and winter, whereas ClAnt demonstrated higher concentrations in the autumn and the winter. ClPhe maintained relatively consistent concentrations across the remaining three seasons. The seasonal characteristics of ClPAHs and BrPAHs (**Fig. 2d**) also differed. Concentrations of BrPAHs varied significantly with the seasons, with no congener detected in the summer and high concentrations of BrPhe, BrAnt, and BrPyr in the spring and winter, likely influenced by climatic conditions such as temperature and sunshine. This disparity can be attributed to the ease of generation from sources and greater atmospheric stability of ClPAHs, while BrPAHs may be subjected to influences from atmospheric processes (Ohura et al. 2009).

Eight meteorological parameters were collected throughout the sampling period: wind speed, wind direction, air pressure, temperature, humidity, total irradiation, sunshine duration, and rainfall. Details

are listed in **Table S5**, and the results of multifactor correlation analysis are shown in **Fig. 2e**. Pearson correlation analysis revealed significant positive correlations between ClPAHs and BrPAHs ($P < 0.001$, $R = 0.96$), PM ($P < 0.01$, $R = 0.96$), and humidity ($P < 0.05$, $R = 0.76$). BrPAHs exhibited a significant positive correlation with humidity ($P < 0.01$, $R = 0.81$). The impact of humidity was notably significant, as an increase in humidity tended to facilitate the upward adsorption of XPAHs onto PM. However, a previous study (Vuong et al. 2020) from Ulsan, South Korea has reported a negative correlation between humidity and XPAHs. This observation suggested that the relationship between XPAHs and humidity varied across different regions. Additionally, ClPAHs shew a significant negative correlation with temperature ($P < 0.01$, $R = –0.90$), suggesting that higher temperatures corresponded to lower ClPAH concentrations. This further elucidated the phenomenon of lower ClPAH levels observed during the summer and autumn seasons. Other meteorological factors didn't show significant correlations with ClPAHs or BrPAHs ($P > 0.05$), possibly due to the intricate interplay of multiple factors under natural conditions. Hence, the specific roles of meteorological conditions such as sunlight intensity, duration of sunshine, temperature, and humidity warranted further investigation.

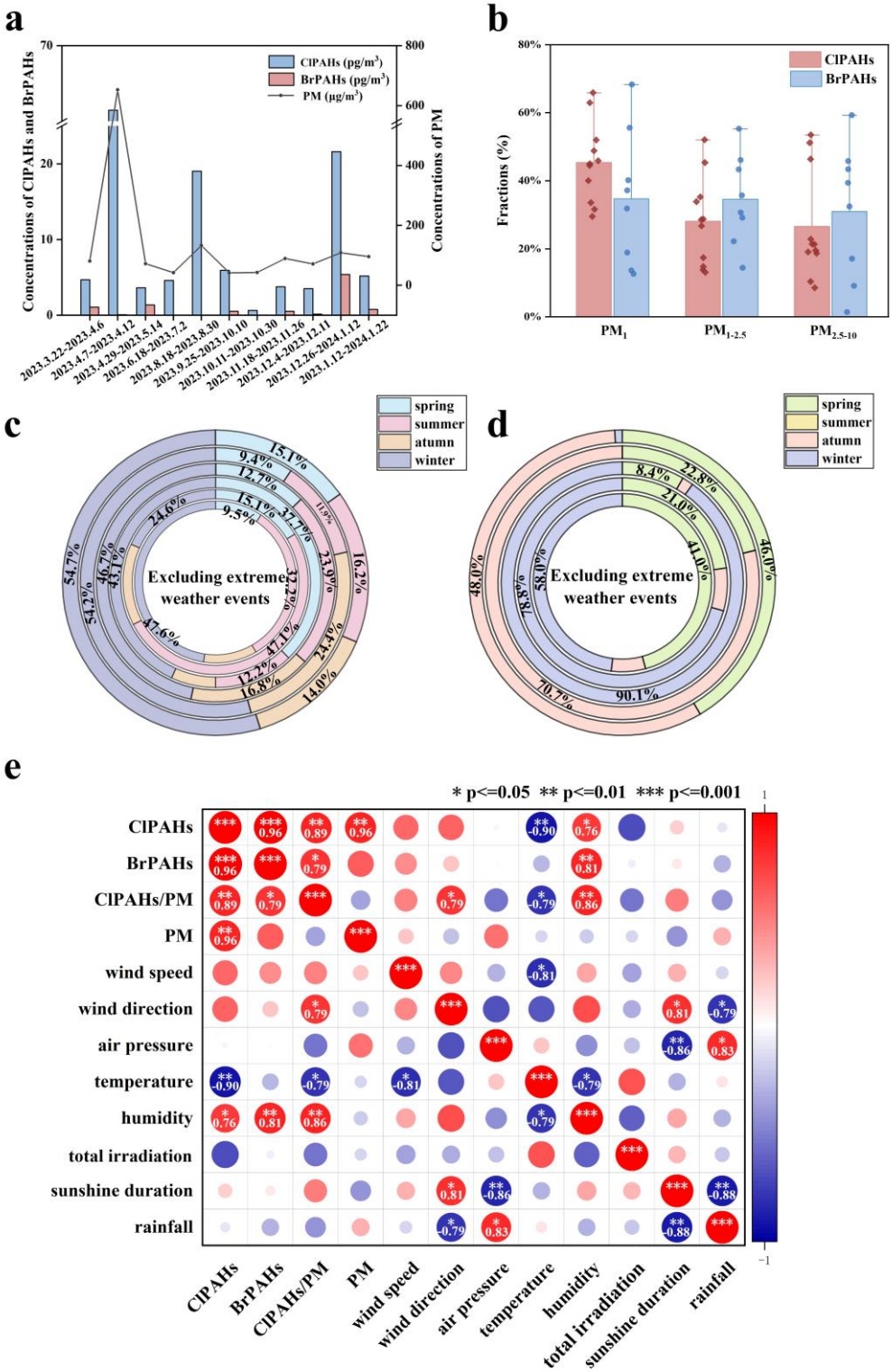

Fig. 2. (a) The fluctuations of concentrations of PM , $\sum_{21}$ClPAHs, and $\sum_{19}$BrPAHs in the atmosphere. (b) The proportions of ClPAHs and BrPAHs across different PM diameters. (c-d) Seasonal distributions of ClPAH (c) and BrPAH (d) congeners, excluding events of extreme conditions, arranged from outermost to innermost layers: ClPhe, ClAnt, ClPyr, ClFluor, ClBaA, and ClBaP; BrPhe, BrAnt, BrPyr, BrTriph, and BrBaA. (e) Pearson correlation analysis between ClPAHs、BrPAHs and ClPAHs/PM with meteorological parameters (wind speed,

wind direction, air pressure, temperature, humidity, total radiation, sunshine duration, and rainfall) under non-extreme weather conditions.

3.3 General transformation mechanisms of particulate XPAHs under photo irradiation

According to both preliminary research(Li et al. 2023) and the experimental results mentioned above, it is evident that meteorological conditions can significantly impact the concentrations and distributions of XPAHs on PM. Controlled laboratory experiments were conducted in this study to unveil the heterogeneous transformation mechanisms of XPAHs.

The transformation ratios of XPAHs were calculated based on the ratios of transformed XPAHs to the initial concentration ($(C_0-C_t)/C_0$). With the increase of irradiation time, a general trend of transformation was observed across XPAH congeners (**Fig. 3)**. Overall, the transformation rates of ClPAHs appeared to follow the sequence: ClPhe < ClFluor < ClPyr <ClBaA ≈ ClAnt < ClBaP (**Fig. S3**). This pattern aligned with the previously reported trends in PAH photolysis rates (Phe < BaA < Ant ≈ BaP) (Zhao et al. 2017), indicating strong influence by the parent PAH structures. In a combined consideration of ClPAHs and their parent PAHs, shown as "ClPAHs+PAHs" in **Fig. S3**, we also observed the formation of PAHs and decreases of total concentrations of ClPAHs and PAHs. This indicated that there were dechlorination of ClPAHs and simultaneous fragmentation of parent PAH structures during the transformation of ClPAHs.

In addition, the substitution numbers in the structures had a strong influence on the transformation of ClPAHs: with increment of the substitution numbers, the transformation ratios progressively decreased (**Fig. 3**). For example, after 1 h of irradiation, transformation ratios were approximately 20% for 3-ClPhe and 2-ClPhe/9-ClPhe, while 10% for 9,10-Cl_2Phe. An exception was observed for ClAnt congeners (1,4-Cl_2Ant or 1,5-Cl_2Ant/9,10-Cl_2Ant < 1-ClAnt/2-ClAnt or 9-ClAnt < 1,5,9,10-Cl_4Ant. This difference could be attributed to the fact that the investigated low-chlorinated ClAnts are dechlorination products of high-chlorinated ClAnts. While the substitution position had some impact, it was not as significant as the number of chlorines. For instance, both 2,5-Cl_2Fluor and 3,8-Cl_2Fluor demonstrate comparable photolysis extents, with approximately 20% transformation after 30 min of irradiation, and transformation ratios of 68.8% and 49.4% after 3 h of irradiation, respectively.

For BrPAHs (**Fig. S4**), the overall transformation ratio ranked as follows: BrPhe < BrAnt < BrPyr ≈ BrFluor < BrBaA < BrBaP. The transformation ratio ranking between BrPAHs and ClPAHs exhibited disparities, implying that distinct halogen substitutions might yield diverse transformation effects.

BrPAHs degraded more rapidly than ClPAHs. For example, BrPyr degraded by 60% after 30 min of irradiation, while ClPyr only degraded by less than 40%. Additionally, the increase in degree of bromination degree didn't appear to have a notable effect on the transformation rate of BrPAHs, which differed from ClPAHs.

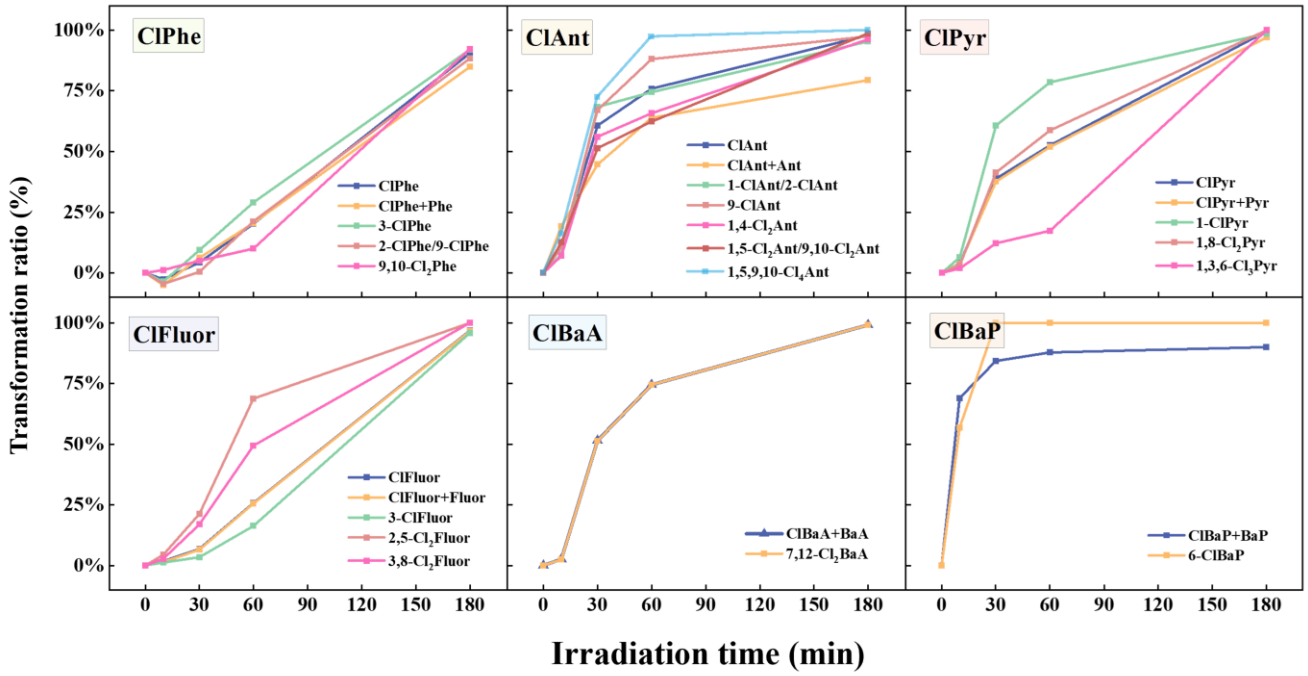

Fig. 3. The relationships between transformation ratios of ClPAHs and photo irradiation time.

3.4 Influencing factors for heterogeneous transformation of particulate XPAHs

The influencing factors, i.e., particle size, relative humidity, reactive oxygen species content, and temperature on XPAH transformation have been investigated (**Text S1**). Although previous studies have revealed variations in XPAH concentrations on particles of different sizes (Jin et al. 2017a; Lara et al. 2022; Ma et al. 2013), the influence of particle size (100 nm, 2 μm, and 10 μm) on transformation efficiency was found to be not notably significant in simulated experiments (**Fig. S5 and Text S3**).

The influence of humidity varied among ClPAHs with different parent structures (**Fig. 4a**). For instance, the transformation of ClPhe and ClFluor slowed down with increasing humidity, whereas the transformation of ClAnt, ClPyr, ClBaA, and ClBaP increased with higher humidity levels, with the highest transformation ratio observed at 45% humidity. Additionally, we found that the impact of humidity on transformation was not consistent for ClPAH congeners in the same homologue groups. For example, transformation of 9,10-Cl_2Phe decreased more sharply than the other ClPhe congeners with the increment of humidity. The combined influence of photo irradiation and humidity enhanced the

transformation of individual ClPAHs (**Fig. S6**). For example, under 45% humidity, ClPyr exhibited an average transformation of 50% in darkness, while this rate increased to 75% under photo irradiation. Possible reasons could be that the addition of photo irradiation drove the formation of hydroxyl radical (·OH), which could participate the breakdown of molecules (Zhang et al. 2023). In contrast, the acceleration of transformation with increasing humidity was relatively universal for BrPAHs, with the most significant effects observed within the 30-45% humidity range (**Fig. S6c** and **Fig. S6d**).

Transformation ratios of XPAHs increased as temperatures rose, with the most significant transformation observed at 30 °C (**Fig. 4b**), indicating that the elevated temperature promote the transformation of XPAHs. The transformation ratio of each congener gradually increased with temperature compared to dark conditions (**Fig. S7a**). Under photo irradiation at the same temperature, the transformation ratios of nearly all XPAH congeners increased by more than 50% compared to dark conditions. This indicated that the breakdown of XPAH molecules was enhanced by the photo irradiation. In both photo irradiation and dark conditions, the transformation ratios of BrPAHs (**Fig. S7c** and **Fig. S7d**) exceeded those of ClPAHs. This phenomenon can be attributed to the differences in bond strength (the bond energy of C-Br is lower at 291 kJ/mol, whereas the bond energy of C-Cl is 345 kJ/mol) (Ohura et al. 2009) and atomic size (the radius of the Cl atom is approximately 99 pm, while the radius of the Br atom is around 114 pm) (Shannon 1976). Adding H_2O_2 to the reaction system simulates the effects of oxidants present in the atmosphere on the impact of XPAH transformation under photochemical conditions. The transformation of ClPAHs accelerated with the increase of H_2O_2 concentration (**Fig. 4c** and **Fig. S8**). TBA was introduced to eliminate the ·OH effect in the control group. Under 1-hour photo irradiation conditions, the transformation rate ranking of ClPAHs is as follows: ClBaP > ClBaA > ClPyr > ClPhe > ClAnt > ClFluor. The transformation of ClFluor showed no significant change with H_2O_2 content, indicating relative stability. Additionally, compared to monochlorinated compounds, the overall transformation ratios of polychlorinated compounds are relatively slower and less influenced by H_2O_2 (except for 1,5,9,10-Cl_4Ant). This also suggested that the dechlorination process was more pronounced in high-chlorinated compounds, while the transformation of low-chlorinated substances was mainly due to ring-opening reactions. The situation was similar for BrPAHs, with transformation rates faster than those of ClPAHs.

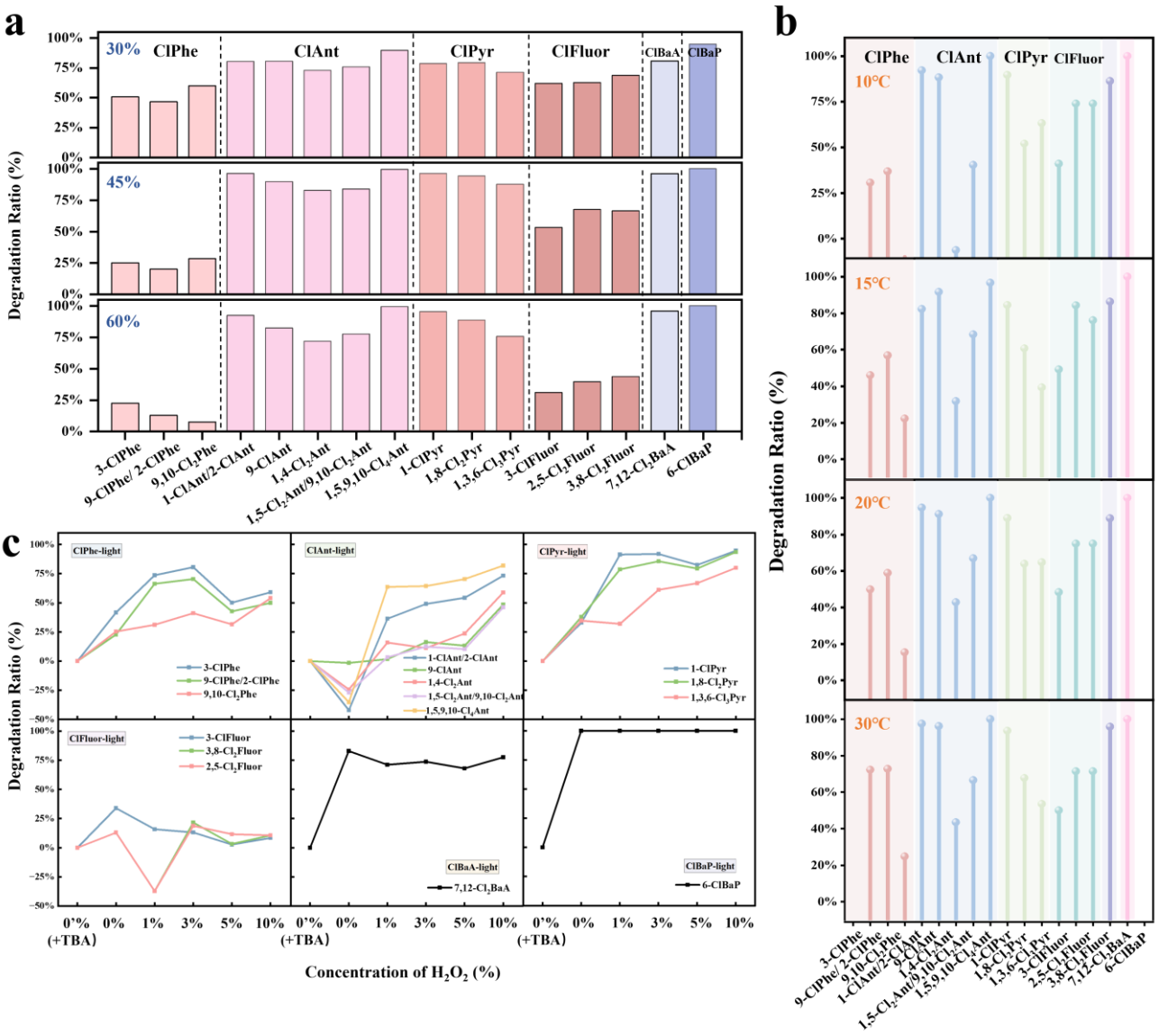

Fig. 4. Transformation ratios of ClPAHs under varying (a) humidity levels, (b) temperature conditions and (c) H_2O_2 concentrations, with photo irradiation.

3.5 Heterogeneous transformation pathways of XPAHs under photo irradiation

According to the results above, there are dechlorination, direct ring-opening, or ring-opening induced by oxidation processes involved in the breakdown of XPAHs. To elucidate the specific transformation pathways of XPAHs, we conducted photolysis experiments on highly chlorinated XPAHs, including 1,4-Cl_2Ant, 9,10-Cl_2Phe, 1,8-Cl_2Pyr, 2,5-Cl_2Fluor, 7,12-Cl_2BaA, and 6-ClBaP, individually. Non-target analysis was then employed to recognize the transformation products of these congeners. Specific mass spectrums can be found in **Fig. S9**, and the relative compounds are listed in **Table S6**. The predominant products were quinones, ketones, hydroxyl-bearing compounds, and ring-opened products, consistent with previous findings on PAH phototransformation products (Jia et al. 2019; Zhao et al.

2017). Surprisingly, no chlorinated oxides were detected. Further analysis of the products from experiments on both ClPAHs and BrPAHs revealed no significant differences. As a result, we confirmed a hypothesis proposed in previous studies (Ohura et al. 2009) that the transformation of XPAHs underwent dehalogenation to form PAHs before oxidation.

The transformation pathways are presented in **Fig. 5**. According to the non-target analysis results of the photolysis products, the primary products for most ClPAHs, with the exception of ClFluor, were the parent PAHs in the initial step. And for ClFluor, the initial step involved not only the dechlorination, but also ring-opening, resulting in the generation of 2,7-dichlorofluorene and 9-chlorofluorene. Research findings suggested that in the atmosphere, the primary reactions for the destruction of aromatic compounds were the addition or substitution with ·OH (Dang et al. 2014). At the same time, the substitution of H or Cl in the main structures of ClPAHs or PAHs by the ·OH could influence the products of the next steps. Therefore, the subsequent steps might include ring opening, oxidation, or hydrolysis.

Specifically, there were three potential pathways for the transformation of 1,4-Cl_2Ant (**Fig. 5a** and **Fig. S9a**). In the first pathway, 1,4-Cl_2Ant could undergo substitution by ·OH to form A2 (1,4-dihydroxyanthracene, $C_{14}H_{10}O_2$), which further oxidized to produce A3 (1,4-anthraquinone, $C_{14}H_8O_2$). For the second and third pathways, 1,4-Cl_2Ant underwent dechlorination to yield A1 (Ant, $C_{14}H_{10}$). The subsequent steps were then similar to those of Ant, with oxidation leading to the formation of A4 (9,10-Anthracenediol, $C_{14}H_{10}O_2$), and further oxidation to A5 (9,10-Anthraquinone, $C_{14}H_8O_2$) as the second pathway. In the third pathway, ring-opening occurred to form A6 (2-Methylnaphthalene, $C_{11}H_{10}$), followed by subsequent chain-breaking ring-opening to form A7 (Nap, $C_{10}H_8$), A8 (1,2,3,4-Tetrahydronaphthalene, $C_{10}H_{12}$), and A9 (2-Methoxyphenol, $C_7H_8O_2$), ultimately yielding A10 (3-Nonanol, $C_9H_{20}O$) and A11 (3-Nonanone, $C_9H_{18}O$). Similar transformation pathways were observed for 9,10-Cl_2Phe (**Fig. 5b** and **Fig. S9b**), 1,8-Cl_2Pyr (**Fig. 5c** and **Fig. S9c**), and 7,12-Cl_2BaA (**Fig. 5e** and **Fig. S9e**), involving dechlorination to generate PAHs, followed by attack by ·OH to produce phenols, further oxidizing to form quinones, acids, and esters. Additionally, 9,10-Cl_2Phe exhibited an additional oxidation pathway involving ring-opening oxidation, yielding B9 (9-Fluorenone, $C_{13}H_8O$), followed by a series of chain-breaking ring-opening reactions to sequentially generate B10 (Benzophenone, $C_{13}H_{10}O$), B11 (3'-Methylacetophenone, $C_9H_{10}O$), and B12 (3-Nonanone, $C_9H_{18}O$). 1,8-Cl_2Pyr also had two additional potential transformation pathways. In the first pathway, uniform cleavage occurred both above

and below the pyrene molecule, generating C4 (Nap, $C_{10}H_8$) and C5 (2-Methylnaphthalene, $C_{11}H_{10}$). In the second pathway, diagonal cleavage resulted in the identification of two products: C6 (2-(2,5-dimethylphenyl)-1,4-dimethylbenzene, $C_{14}H_{14}$) and C7 (4,4'-Dimethyldiphenyl, $C_{14}H_{14}$). C6 underwent attack by ·OH/O_2^- radicals to ultimately form C8 (Benzophenone, $C_{13}H_{10}O$), followed by further ring-opening cleavage to produce C9 (3'-Methylacetophenone, $C_9H_{10}O$). Similarly, C10 (2-Phenylprocpionaldehyde, $C_9H_{10}O$) was formed by oxidation-induced chain-breaking of C8.

For ClFluor (**Fig. 5d** and **Fig. S9d**), the initial step involved ring-opening, generating D1 (2,7-Cl_2Fle, $C_{13}H_8Cl_2$) and D2 (9-ClFle, $C_{13}H_9Cl$). Subsequent dechlorination and ring-opening led to the formation of D3 (4,4'-Dimethyldiphenyl, $C_{14}H_{14}$), D4 (2-(2,5-dimethylphenyl)-1,4-dimethylbenzene, $C_{14}H_{14}$), and D5 (Benzophenone, $C_{13}H_{10}O$) in the samples. In the second pathway, the initial dechlorination process resulted in the formation of D6 (Fluor, $C_{16}H_{10}$), which yielded D7 (1H-Indene, 2,3-dihydro-4,7-dimethyl-, $C_{11}H_{14}$) and D9 (Nap, $C_{10}H_8$). D7 underwent bond cleavage to form D8 (1H-Indene, octahydro-, C_9H_{16}), while D10 (1,2-Diethylbenzene, $C_{10}H_{14}$) was the ring-opening product of D9. Further oxidation (alcohol to aldehyde) sequentially yielded D11 (1,2-Dicarboxybenzene, $C_8H_6O_4$) and D12 (Dibutyl phthalate, $C_{16}H_{22}O_4$).

6-ClBaP, as a mono-chlorinated compound (**Fig. 5f** and **Fig. S9f**), exhibited the highest phototransformation ratio among all ClPAH congeners. After dechlorination, the initial step generated F1 (BaP, $C_{20}H_{12}$). Among them, positions 3, 6, and 12 of BaP were particularly reactive, and ·OH attacks led to the formation of F2, F3, and F4 (6-Benzo[a]pyrenol, 6,12-Dihydroxybenzo[a]pyrene, and 9,12-Dihydroxybenzo[a]pyrene, $C_{20}H_{12}O$), subsequently further generated F5, F6 and F7 (6-Benz[a]pyrenone, Benzo[a]pyrene-6,12-dione, and Benzo[a]pyrene-3,6-dione, $C_{20}H_{10}O_2$). Under light exposure, F6 underwent further oxidation and ring-opening to produce F8 (Lapachol, $C_{15}H_{14}O_3$), F9 (2,6-Diisopropylnaphthalene, $C_{16}H_{20}$), and F11 (Dimethyl phthalate, $C_{16}H_{22}O_4$), as reported by S. Zhao et al (Zhang et al. 2023). The exploration of XPAH transformation is limited by the absence of quantification of the products. Further studies are necessary to elucidate the specific molecular assignments.

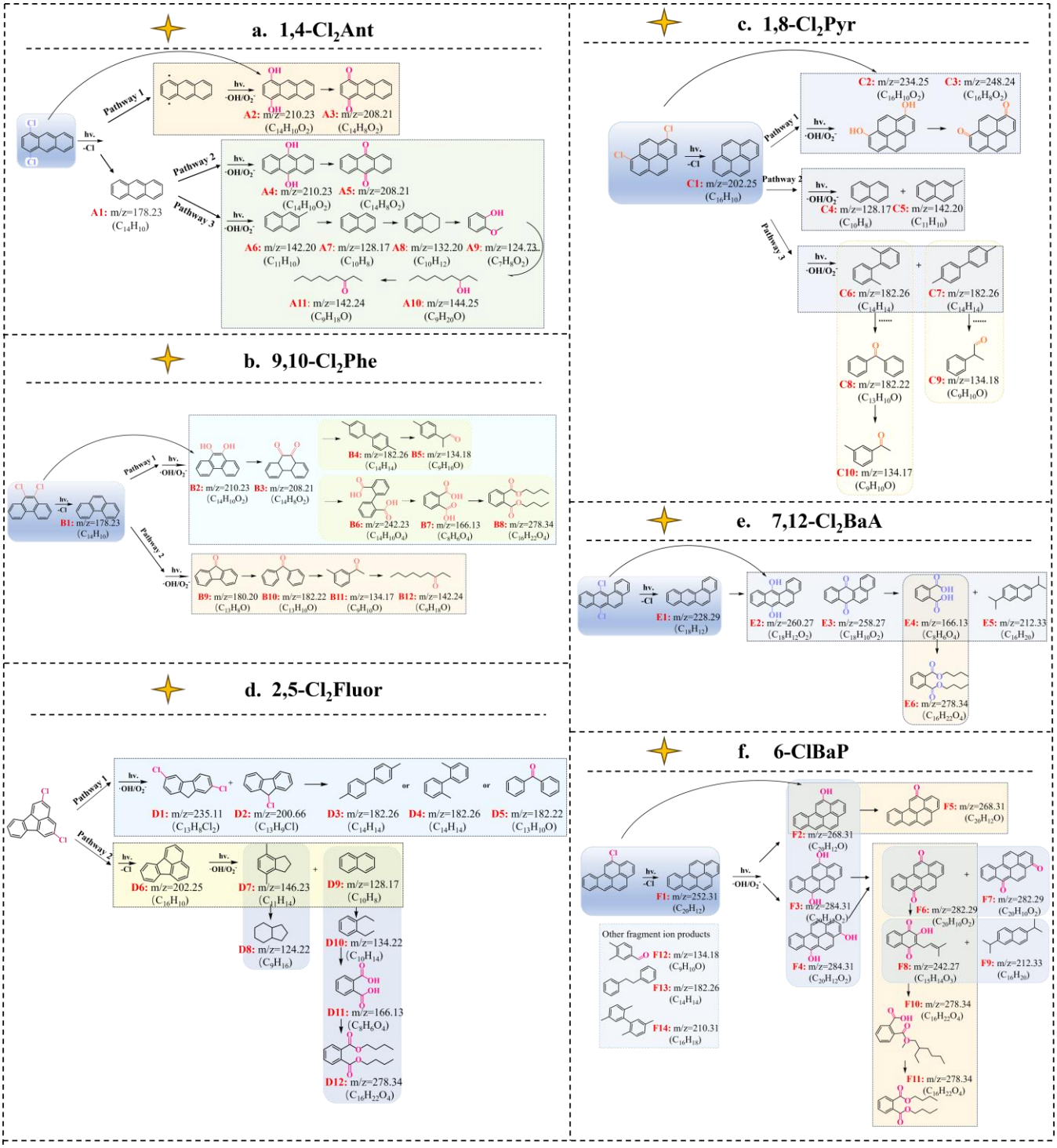

Fig. 5. (a-f) The transformation pathways and relative products of ClPAHs. ((a) 1,4-Cl_2Ant; (b) 9,10-Cl_2Phe; (c) 1,8-Cl_2Pyr; (d) 2,5-Cl_2Fluor; (e) 7,12-Cl_2BaA; (f) 6-ClBaP).

3.6 Assessments of persistence, bioaccumulation, long-range transportation and toxicities of XPAHs and their transformation products

Studies have suggested that transformation products of organic pollutants might exhibit distinct environmental behaviors and heightened ecological toxicity (Zhang et al. 2023). For the assessed P-B-

LRTP scores of XPAHs and their transformation products in this study (**Fig. 6a** and **Table S6**), it could be observed that as the transformation pathways progressed, the scores of the transformation products decreased. For instance, the score of 9,10-Cl_2Phe was 5.07, which decreased to 2.13 after dechlorination, and further oxidation products have even lower scores ranging from 1.65 to -1.27 (9,10-Difluorenquinone to 1,2-Benzenedicarboxylic acid). However, there were also transformation products with relatively high scores, such as B9 (9H-Fluorene-9-one, score: 1.57) and B10 (Benzophenone, score: 1.81), which warrant special attention in future studies.

To further investigate the toxicities of these transformation products, the lethal doses (LD50) and toxicity levels (**Fig. 6b** and **Table S7**) were prediectd by the respiratory toxicity model in ProTox 3.0 (Banerjee et al. 2024). The findings indicated that as the transformation pathways progressed, the LD50 values of the products generally increased, except for 2,5-Cl_2Fluor, indicating a general toxicity decrement alongside XPAH transformation. For instance, the LD50 of 9,10-Cl_2Phe was 886 mg/kg with a toxicity level of 4. Among its transformation products, only B1 (Phe) had an LD50 (316 mg/kg, level 4) lower than that of 9,10-Cl_2Phe, while the toxicities of other oxidation and ring-opening products were lower. However, previous studies on the aryl hydrocarbon receptor activities of XPAHs in yeast assays reported the opposite results on toxicities of 9,10-Cl_2Phe and Phe: the relative equivalent potency of 9,10-Cl_2Phe was found to be much higher than Phe. In the case of 2,5-Cl_2Fluor, its inherently high LD50 (4220 mg/kg, level 5) resulted in most of its products having higher toxicity levels compared to the parent compound. Overall, most transformation products have toxicity levels lower than their precursors. However, given the disparities between model predictions and experimental results, further toxicity experiments are needed to substantiate the changes in toxicity during the transformation process of XPAHs.

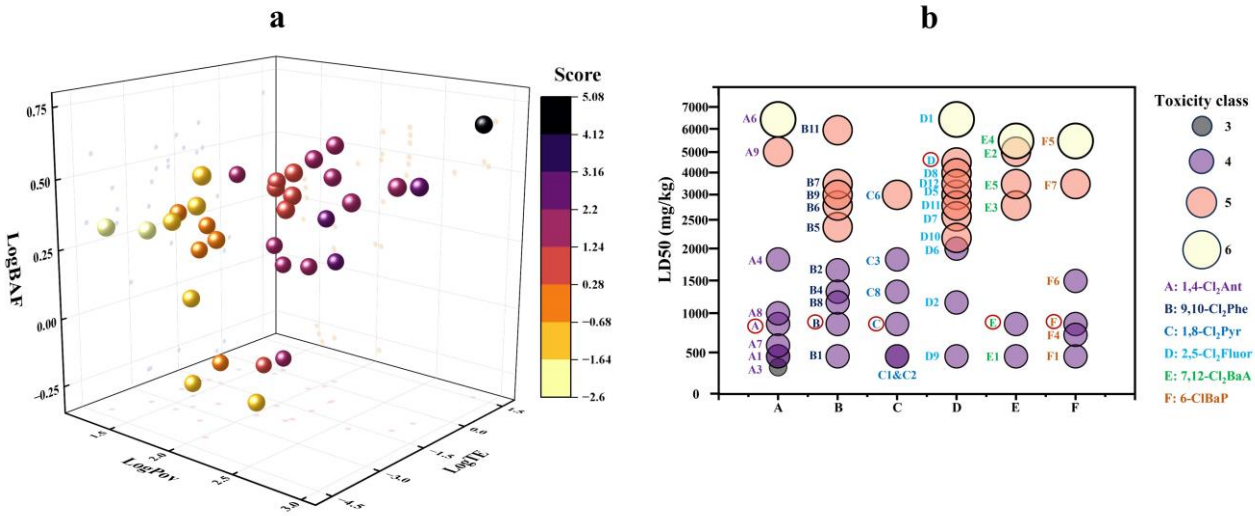

Fig. 6. (a) Prediction of environmental behaviors of XPAHs and their transformation products. (b) Respiratory toxicities (LD50) of XPAHs and their transformation products predicted by ProTox 3.0 model.

4. Conclusion

In summary, this study elucidated the mechanisms, influencing factors, pathways, and products involved in the conversion of XPAHs on PM through comprehensive field sampling and laboratory simulations. Experimental findings revealed that the molecular structures of PAHs exerted a significant influence on the conversion process, with dehalogenation and cleavage of the parent ring structure being prominent features of XPAHs conversion. The number and position of substituents further modulated the conversion dynamics. Key environmental parameters, including humidity, temperature, and H_2O_2 concentration, were identified as critical factors impacting conversion efficiency. The resulting conversion products and pathways were systematically hypothesized and confirmed, indicating a progressive decrease in environmental risks associated with the products as conversion advanced. This study provided novel insights into the heterogeneous conversion mechanisms of XPAHs on particulate matter, offering valuable contributions to the understanding of their environmental behavior and impact.

ASSOCIATED CONTENT

Author contributions

YY, RJ and MZ conceived the study and wrote the paper, YY, YL, GZ, SZ and XL performed the measure ments and collected data. All authors contributed to the data analysis and review of the paper.

Competing Interests

he authors declare that they have no conflict of interest.

Data availability

All data are available from the authors upon request by contacting Rong Jin (jinrong@ucas.ac.cn).

Supporting information

Including detailed information on chemicals, sample testing and analysis data, screening of chemical properties and toxicity prediction information, relevant parameters and data from simulation experiments, as well as chromatograms for product identification.

Acknowledgement

The authors acknowledge the financial support provided by the Natural Science Foundation of Zhejiang Province (Grant No. LQ22B070009), the National Natural Science Foundation of China (Grant No. 22106030), "Pioneer" and "Leading Goose" R&D Program of Zhejiang (Grant No. 2023C03157) and the Research Funds of Hangzhou Institute for Advanced Study, UCAS (Grant No. 2023HIAS-Y014, 2022ZZ01017).

References

Banerjee, P.; Kemmler, E.; Dunkel, M.; Preissner, R., 2024. ProTox 3.0: a webserver for the prediction of toxicity of chemicals. Nucleic Acids Res 10.1093/nar/gkae303

Cao, Q.; Liu, Y.; Lyu, K.; Yu, Y.; Li, D.H.W.; Yang, L., 2020. Solar Radiation Zoning and Daily Global Radiation Models for Regions with Only Surface Meteorological Measurements in China. Energ Convers Manage 225, 10.1016/j.enconman.2020.113447

Concha, C.; Manzano, C.A., 2023. Priority pesticides in Chile: Predicting their environmental distribution, bioaccumulation, and transport potential. Integr Environ Assess Manag 19, 676-683. 10.1002/ieam.4680

Dang, J.; Shi, X.; Zhang, Q.; Hu, J.; Chen, J.; Wang, W., 2014. Mechanistic and Kinetic Studies on the OH-Initiated Atmospheric Oxidation of Fluoranthene. Sci Total Environ 490, 639-646. 10.1016/j.scitotenv.2014.04.134

Deng, Q.X.; Feng, J.R.; Gao, P.P.; Ni, H.G., 2023. Combined effects of vehicles and waste incineration on urban air halogenated and parent polycyclic aromatic hydrocarbons. Environ Int 171, 107720. 10.1016/j.envint.2022.107720

Hu, W.; Liu, D.; Su, S.; Ren, L.; Ren, H.; Wei, L.; Yue, S.; Xie, Q.; Zhang, Z.; Wang, Z.; Yang, N.; Wu, L.; Deng, J.; Qi, Y.; Fu, P., 2021. Photochemical Degradation of Organic Matter in the Atmosphere. Adv Sustain Syst 5, 10.1002/adsu.202100027

Jia, H.; Zhao, S.; Shi, Y.; Zhu, K.; Gao, P.; Zhu, L., 2019. Mechanisms for Light-Driven Evolution of Environmentally Persistent Free Radicals and Photolytic Degradation of PAHs on Fe(III)-Montmorillonite Surface. J Hazard Mater 362, 92-98. 10.1016/j.jhazmat.2018.09.019

Jin, R.; Liu, G.; Jiang, X.; Liang, Y.; Fiedler, H.; Yang, L.; Zhu, Q.; Xu, Y.; Gao, L.; Su, G.; Xiao, K.; Zheng, M., 2017a. Profiles, Sources and Potential Exposures of Parent, Chlorinated and Brominated Polycyclic Aromatic Hydrocarbons in Haze Associated Atmosphere. Sci Total Environ 593-594, 390-398. 10.1016/j.scitotenv.2017.03.134

Jin, R.; Liu, G.; Zheng, M.; Jiang, X.; Zhao, Y.; Yang, L.; Wu, X.; Xu, Y., 2017b. Secondary Copper Smelters as Sources of Chlorinated and Brominated Polycyclic Aromatic Hydrocarbons. Environ Sci Technol 51, 7945-7953. 10.1021/acs.est.7b02031

Jin, R.; Liu, G.; Zhou, X.; Zhang, Z.; Lin, B.; Liu, Y.; Qi, Z.; Zheng, M., 2023. Analysis of Polycyclic Aromatic Hydrocarbon Derivatives in Environment. Trac-Trend anal chem 160, 10.1016/j.trac.2023.116942

Jin, R.; Yang, L.; Zheng, M.; Xu, Y.; Li, C.; Liu, G., 2018. Source identification and quantification of chlorinated and brominated polycyclic aromatic hydrocarbons from cement kilns co-processing solid wastes. Environ Pollut 242, 1346-1352. 10.1016/j.envpol.2018.08.025

Jin, R.; Zheng, M.; Lammel, G.; Bandowe, B.A.M.; Liu, G., 2020. Chlorinated and Brominated Polycyclic Aromatic Hydrocarbons: Sources, Formation Mechanisms, and Occurrence in the Environment. Prog Energy Combust Sci 76, 10.1016/j.pecs.2019.100803

Jin, R.; Zheng, M.; Yang, H.; Yang, L.; Wu, X.; Xu, Y.; Liu, G., 2017c. Gas–particle phase partitioning and particle size distribution of chlorinated and brominated polycyclic aromatic hydrocarbons in haze. Environmental Pollution 231, 1601-1608. 10.1016/j.envpol.2017.09.066

Kakimoto, K.; Nagayoshi, H.; Konishi, Y.; Kajimura, K.; Ohura, T.; Hayakawa, K.; Toriba, A., 2014. Atmospheric chlorinated polycyclic aromatic hydrocarbons in East Asia. Chemosphere 111, 40-46. 10.1016/j.chemosphere.2014.03.072

Kang, Q.; Bao, S.; Chen, B., 2021. Phototransformation of Three Polychlorinated Naphthalenes on

508 Surface of Atmospheric Particulate Matter. J Hazard Mater 409, 124895.
509 10.1016/j.jhazmat.2020.124895
510 Kitazawa, A.; Amagai, T.; Ohura, T., 2006. Temporal Trends and Relationships of Particulate
511 Chlorinated Polycyclic Aromatic Hydrocarbons and Their Parent Compounds in Urban Air.
512 Environ Sci Technol 40, 4592-4598.
513 Lara, S.; Villanueva, F.; Martín, P.; Salgado, S.; Moreno, A.; Sánchez-Verdú, P., 2022. Investigation of
514 PAHs, Nitrated PAHs and Oxygenated PAHs in PM10 Urban Aerosols. A Comprehensive Data
515 Analysis. Chemosphere 294, 10.1016/j.chemosphere.2022.133745
516 Laskin, A.; Laskin, J.; Nizkorodov, S.A., 2015. Chemistry of Atmospheric Brown Carbon. Chem Rev
517 115, 4335-4382. 10.1021/cr5006167
518 Li, X.; Abdullah, L.C.; Sobri, S.; Md Said, M.S.; Hussain, S.A.; Aun, T.P.; Hu, J., 2023. Long-Term Air
519 Pollution Characteristics and Multi-scale Meteorological Factor Variability Analysis of Mega-
520 mountain Cities in the Chengdu-Chongqing Economic Circle. Water Air Soil Pollut 234, 328.
521 10.1007/s11270-023-06279-8
522 Liu, Q.; Liggio, J.; Li, K.; Lee, P.; Li, S.M., 2019a. Understanding the Impact of Relative Humidity and
523 Coexisting Soluble Iron on the OH-Initiated Heterogeneous Oxidation of Organophosphate
524 Flame Retardants. Environ Sci Technol 53, 6794-6803. 10.1021/acs.est.9b01758
525 Liu, Q.; Xu, X.; Wang, L.; Lin, L.; Wang, D., 2019b. Simultaneous Determination of Forty-Two Parent
526 and Halogenated Polycyclic Aromatic Hydrocarbons Using Solid-Phase Extraction Combined
527 with Gas Chromatography-Mass Spectrometry in Drinking Water. Ecotoxicol Environ Saf 181,
528 241-247. 10.1016/j.ecoenv.2019.06.011
529 Ma, J.; Chen, Z.; Wu, M.; Feng, J.; Horii, Y.; Ohura, T.; Kannan, K., 2013. Airborne PM2.5/PM10-
530 Associated Chlorinated Polycyclic Aromatic Hydrocarbons and Their Parent Compounds in a
531 Suburban Area in Shanghai, China. Environ Sci Technol 47, 7615-7623. 10.1021/es400338h
532 Malecha, K.; Nizkorodov, S., 2016. Photodegradation of Secondary Organic Aerosol Particles as a
533 Source of Small, Oxygenated Volatile Organic Compounds. Environ Sci Technol 50, 9990-9997.
534 10.1021/acs.est.6b02313
535 Nilsson, U.L.; Ostman, C.E., 1993. CHLORINATED POLYCYCLIC AROMATIC-HYDROCARBONS
536 - METHOD OF ANALYSIS AND THEIR OCCURRENCE IN URBAN AIR. Environmental
537 Science & Technology 27, 1826-1831. 10.1021/es00046a010
538 Nishimura, C.; Horii, Y.; Tanaka, S.; Asante, K.A.; Ballesteros, F., Jr.; Viet, P.H.; Itai, T.; Takigami, H.;
539 Tanabe, S.; Fujimori, T., 2017. Occurrence, Profiles, and Toxic Equivalents of Chlorinated and
540 Brominated Polycyclic Aromatic Hydrocarbons in E-Waste Open Burning Soils. Environ Pollut
541 225, 252-260. 10.1016/j.envpol.2016.10.088
542 Noro, K.; Omagari, R.; Ito, K.; Wang, Q.; Sei, K.; Miyake, Y.; Amagai, T., 2023. Sampling, Pretreatment,
543 Instrumental Analysis, and Observed Concentrations of Polycyclic Aromatic Hydrocarbons,
544 Polychlorinated Naphthalenes, and Halogenated Polycyclic Aromatic Hydrocarbons: A Review.
545 Trac-Trend anal chem 169, 10.1016/j.trac.2023.117384
546 Ohura, T.; Amagai, T.; Makino, M., 2008. Behavior and Prediction of Photochemical Degradation of
547 Chlorinated Polycyclic Aromatic Hydrocarbons in Cyclohexane. Chemosphere 70, 2110-2117.
548 10.1016/j.chemosphere.2007.08.064
549 Ohura, T.; Horii, Y.; Kojima, M.; Kamiya, Y., 2013. Diurnal Variability of Chlorinated Polycyclic
550 Aromatic Hydrocarbons in Urban Air, Japan. Atmos Environ 81, 84-91.
551 10.1016/j.atmosenv.2013.08.044
552 Ohura, T.; Morita, M.; Makino, M.; Amagai, T.; Shimoi, K., 2007. Aryl Hydrocarbon Receptor-Mediated

553 Effects of Chlorinated Polycyclic Aromatic Hydrocarbons. Chem Res Toxicol 20, 1237–1241.
554 Ohura, T.; Sakakibara, H.; Watanabe, I.; Shim, W.J.; Manage, P.M.; Guruge, K.S., 2015. Spatial and
555 vertical distributions of sedimentary halogenated polycyclic aromatic hydrocarbons in
556 moderately polluted areas of Asia. Environ Pollut 196, 331-340. 10.1016/j.envpol.2014.10.028
557 Ohura, T.; Savada, K.; Amagai, T.; Shinomiya, M., 2009. Discovery of Novel Halogenated Polycyclic
558 Aromatic Hydrocarbons in Urban Particulate Matters: Occurrence, Photostability, and AhR
559 Activity. Environ Sci Technol 43, 2269–2275.
560 Sei, K.; Wang, Q.; Tokumura, M.; Miyake, Y.; Amagai, T., 2021. Accurate and Ultrasensitive
561 Determination of 72 Parent and Halogenated Polycyclic Aromatic Hydrocarbons in a Variety of
562 Environmental Samples via Gas Chromatography-Triple Quadrupole Mass Spectrometry.
563 Chemosphere 271, 129535. 10.1016/j.chemosphere.2021.129535
564 Shannon, R.D., 1976. Revised effective ionic radii and systematic studies of interatomic distances in
565 halides and chalcogenides. Acta Crystallographica Section A 32, 751-767.
566 10.1107/s0567739476001551
567 Shiraishi, H.; Pilkington, N.H.; Otsuki, A.; Fuwa, K., 1985. Occurrence of chlorinated polynuclear
568 aromatic hydrocarbons in tap water. Environ Sci Technol 19, 585-590. 10.1021/es00137a001
569 Shiraiwa, M.; Ammann, M.; Koop, T.; Pöschl, U., 2011. Gas uptake and chemical aging of semisolid
570 organic aerosol particles. Proc Natl Acad Sci USA 108, 11003-11008. 10.1073/pnas.1103045108
571 Sun, J.L.; Zeng, H.; Ni, H.G., 2013. Halogenated polycyclic aromatic hydrocarbons in the environment.
572 Chemosphere 90, 1751-1759. 10.1016/j.chemosphere.2012.10.094
573 Takikawa, T.; Wang, Q.; Omagari, R.; Noro, K.; Miyake, Y.; Amagai, T., 2023. Development of an
574 Analytical Method for Indoor Polycyclic Aromatic Hydrocarbons and Their Halogenated
575 Derivatives by Using Thermal Separation Probe Coupled to Gas Chromatography-Tandem Mass
576 Spectrometry. Sci Total Environ 903, 166931. 10.1016/j.scitotenv.2023.166931
577 Vuong, Q.T.; Thang, P.Q.; Nguyen, T.N.T.; Ohura, T.; Choi, S.-D., 2020. Seasonal variation and
578 gas/particle partitioning of atmospheric halogenated polycyclic aromatic hydrocarbons and the
579 effects of meteorological conditions in Ulsan, South Korea. Environmental Pollution 263,
580 10.1016/j.envpol.2020.114592
581 Wang, T.; Liu, Y.; Deng, Y.; Cheng, H.; Yang, Y.; Feng, Y.; Zhang, L.; Fu, H.; Chen, J., 2020.
582 Photochemical Oxidation of Water-Soluble Organic Carbon (WSOC) on Mineral Dust and
583 Enhanced Organic Ammonium Formation. Environ Sci Technol 54, 15631-15642.
584 10.1021/acs.est.0c04616
585 Wang, Y.; Su, P.; Ge, X.; Ren, H.; Ma, S.; Shen, G.; Chen, Q.; Yu, Y.; An, T., 2022. Identification of
586 specific halogenated polycyclic aromatic hydrocarbons in surface soils of petrochemical, flame
587 retardant, and electronic waste dismantling industrial parks. J Hazard Mater 436, 129160.
588 10.1016/j.jhazmat.2022.129160
589 Xia, Z.; Idowu, I.; Marvin, C.; Thomas, P.J.; Johnson, W.; Francisco, O.; Stetefeld, J.; Crimmins, B.; Fry,
590 M.; Tomy, G.T., 2019. Identification of halogenated polycyclic aromatic hydrocarbons in
591 biological samples from Alberta Oil-Sands Region. Chemosphere 215, 206-213.
592 10.1016/j.chemosphere.2018.10.050
593 Xie, J.; Tao, L.; Wu, Q.; Lei, S.; Lin, T., 2021. Environmental Profile, Distributions and Potential
594 Sources of Halogenated Polycyclic Aromatic Hydrocarbons. J Hazard Mater 419,
595 10.1016/j.jhazmat.2021.126164
596 Yang, L.; Shen, J.; Zheng, M.; Yang, Q.; Li, D.; Liu, G., 2022a. Occurrence of chlorinated and
597 brominated polycyclic aromatic hydrocarbons from electric arc furnace for steelmaking. Environ

Pollut 294, 118663. 10.1016/j.envpol.2021.118663
Yang, Y.; Liu, G.; Zheng, M.; Liu, S.; Yang, Q.; Liu, X.; Wang, M.; Yang, L., 2022b. Discovery of significant atmospheric emission of halogenated polycyclic aromatic hydrocarbons from secondary zinc smelting. Ecotoxicol Environ Saf 238, 113594. 10.1016/j.ecoenv.2022.113594
Zhang, L.; Yan, W.; Kohtani, S.; Fukuyoshi, S.; Hu, M.; Nagao, S.; Tang, N., 2024. Promotive Effects of Marine-Derived Dimethyl Sulfoxide on the Photodegradation of Phenanthrene in the Atmosphere. Sci Total Environ 926, 171938. 10.1016/j.scitotenv.2024.171938
Zhang, L.H.; Li, P.J.; Gong, Z.Q.; Oni, A.A., 2006. Photochemical behavior of benzo[a]pyrene on soil surfaces under UV light irradiation. J Environ Sci (China) 18, 1226-1232. 10.1016/s1001-0742(06)60067-3
Zhang, Q.; Wang, Y.; Gao, M.; Li, Y.; Zhao, L.; Yao, Y.; Chen, H.; Wang, L.; Sun, H., 2023. Organophosphite Antioxidants and Novel Organophosphate Esters in Dust from China: Large-Scale Distribution and Heterogeneous Phototransformation. Environ Sci Technol 57, 4187-4198. 10.1021/acs.est.2c08239
Zhao, S.; Jia, H.; Nulaji, G.; Gao, H.; Wang, F.; Wang, C., 2017. Photolysis of Polycyclic Aromatic Hydrocarbons (PAHs) on Fe($^{3+}$)-Montmorillonite Surface Under Visible Light: Degradation Kinetics, Mechanism, and Toxicity Assessments. Chemosphere 184, 1346-1354. 10.1016/j.chemosphere.2017.06.106
Zhu, J.; Sheng, M.; Shang, J.; Kuang, Y.; Shi, X.; Qiu, X., 2022. Photocatalytic Role of Atmospheric Soot Particles under Visible-Light Irradiation: Reactive Oxygen Species Generation, Self-Oxidation Process, and Induced Higher Oxidative Potential and Cytotoxicity. Environ Sci Technol 56, 7668-7678. 10.1021/acs.est.2c00420